Journal of Micromechanics and Microengineering

PAPER

Metrology and characterization of SU-8 microstructures using autofluorescence emission

To cite this article: Pradeep Kumar Ramkumar *et al* 2021 *J. Micromech. Microeng.* **31** 045014

IOP Publishing Journal of Micromechanics and Microengineering
J. Micromech. Microeng. **31** (2021) 045014 (11pp) https://doi.org/10.1088/1361-6439/abe7c9

Metrology and characterization of SU-8 microstructures using autofluorescence emission

Pradeep Kumar Ramkumar[1], **Corey M Rountree**[1], **Laxman Saggere**[2] **and John D Finan**

Department of Mechanical and Industrial Engineering, University of Illinois at Chicago, Chicago, IL 60607, United States of America

E-mail: jdfinan@uic.edu

Received 3 September 2020, revised 19 January 2021
Accepted for publication 18 February 2021
Published 3 March 2021

Abstract

Sophisticated three-dimensional microstructures fabricated using the negative tone SU-8 photoresist are used in many biomedical and microfluidic applications. Scanning electron microscopy (SEM) and profilometry are commonly used metrological techniques for the dimensional characterization of fabricated SU-8 microstructures but are not viable for non-destructive measurements and characterization of subsurface features like hidden microchannels. In this study, we report a unique methodology for the non-destructive dimensional characterization of SU-8 microstructures using the emitted autofluorescence radiation from fabricated SU-8 microstructures to generate depth profiles. The relationship between autofluorescence emission intensities and the thicknesses of the microstructures measured using SEM was determined and used to characterize the dimensions of unknown SU-8 microstructures based on their autofluorescence intensities. Lateral dimensions were also measured. This relationship was used to create highly accurate depth profiles for different types of microstructures including hidden subsurface features. These results were validated by comparison with SEM. The results suggest a feasible and accurate non-destructive, low cost, metrological technique to characterize SU-8 surface and subsurface microstructures using autofluorescence emission intensities.

Keywords: SU-8, autofluorescence, metrology, imaging

(Some figures may appear in colour only in the online journal)

1. Introduction

The negative photoresist SU-8 has become a widely used structural material for fabricating microelectromechanical systems (MEMS) devices for a variety of applications including biomedical diagnostics with lab-on-a-chip designs, manipulating small volume fluid flow using microfluidics, and hermetic packaging for implantable devices [1–5]. The increasing demand for SU-8 in MEMS devices is in large part due to its range of desirable properties which include optical transparency, biocompatibility, ease of fabrication, and mechanical strength. However, one potential limitation of SU-8 for MEMS applications is the relatively high autofluorescence emissions observed at visible wavelengths, which can interfere or mask detection of fluorescent dyes and probes for biological MEMS (Bio-MEMS) applications [6–9]. Although research has been directed towards reducing SU-8 autofluorescence, it has proven difficult to eliminate entirely since the level of autofluorescence emission is directly proportional to the thickness of SU-8 [9]. While SU-8's high autofluorescence emission limits its applications for fluorescence-based Bio-MEMS, it has untapped potential as an imaging and metrology technique for measuring SU-8 dimensions.

[1] These authors contributed equally to the work.
[2] This author is now deceased.

Metrology is a critical step in the SU-8 microfabrication process where imaging or other measurement tools are used to inspect and validate the dimensional accuracy of SU-8 microstructures. Recent advances in grayscale SU-8 photolithography make this step particularly important since it facilitates microfabrication of complex three-dimensional (3D) microstructures containing enclosed microchannels and other hidden subsurface features [10]. Despite the widespread usage of SU-8 for MEMS applications, a limited number of metrology techniques have been employed. Most commonly, scanning electron microscopy (SEM) and optical profilometry have been utilized for determining the thickness and lateral dimensions of SU-8 microstructures. These methods provide high-resolution measurements for simple microstructures but cannot measure the thicknesses of complex 3D microstructures with hidden features without destructive sectioning. Here, we propose fluorescence microscopy as an alternative metrology technique offering advantages over existing SU-8 metrology methods.

In this work, we present a novel method for using SU-8's inherent autofluorescence emission as a metrology technique to measure the thickness and lateral dimensions of SU-8 microstructures. Using a conventional fluorescence microscope, we imaged 3D SU-8 microstructures with a standard DAPI filter set (peak excitation wavelength of 365 nm; peak emission wavelength of 440 nm) and modeled the relationship between SU-8 thickness and the resulting autofluorescence emission intensity with a variation of Beer–Lambert's Law. We also characterized lateral dimensions using the autofluorescence emission image profiles. We then validated these estimated thickness and lateral dimensions with results obtained from SEM imaging as part of blinded experiments. In comparison with existing techniques, our low-cost method allows fast topological identification and thickness measurement of 3D microstructures *in-situ* without destructive sectioning since it measures emitted light radiation instead of the reflected light. This measurement of emitted radiation enables the non-destructive characterization of surface as well as subsurface features in microstructures, which is impossible with other existing techniques like optical profilometry or SEM. In the following sections, we report the methodology and results for autofluorescence emission measurement of SU-8 samples verified with data from SEM imaging.

2. Methods

The autofluorescence emission-based metrology technique required the following five steps. The first step was the microfabrication of the samples on borosilicate glass substrates. The second step involved the fabrication of the samples on silicon substrates. Glass and silicon substrates were chosen to test the reliability of the technique on both transparent and opaque substrates. The samples included semicircular pyramidal structures and hidden subsurface structures. The next step was to image the autofluorescence emission of these samples by capturing the response to UV radiation generated from an epi-fluorescence illuminator. The third step was the determination of feature size using SEM to measure both the lateral dimensions and the thickness of the SU-8 samples. The fourth step determined the relationship between the pixel intensities and their corresponding feature sizes from SEM. The autofluorescence emission images were converted into 2D depth profile images using these relationships. The 2D depth profile images were generated for different SU-8 microstructures of different feature sizes using this predetermined relationship between pixel intensities and the SEM feature sizes. Finally, we validated the results obtained from our technique by comparing it with the dimensions measured using the SEM micrographs. Our technique was used to characterize the thickness and lateral dimensions of suspended bridge structures fabricated on silicon substrates. The results were compared with those obtained from SEM micrographs as part of blinded experiments.

2.1. Fabrication of the samples on borosilicate glass substrates

SU-8 semicircular pyramidal structures and hidden subsurface microstructures were fabricated in a class 1000 cleanroom using a laser-based maskless pattern generator. The exposed designs are depicted in figure 1. Successive multi-step spin coating and exposure was used to create a semicircular pyramidal structure of different heights. Hidden subsurface features were fabricated using grayscale lithography. These hidden subsurface features consist of interconnected microwells as depicted in figure 1(b). The process is described in detail below.

Borosilicate glass wafers were cleaned by sequential immersion in baths of acetone, methanol, and isopropanol. The wafer was then dehydration baked at 200 °C for 30 min using a programmable hot plate (Brewer Science 1300X, Brewer Science, Rolla, MO, USA). A 100 nm layer of Omnicoat (Microchem, Westborough, MA, USA) adhesion promoter was spin coated using a programmable spin coater. The wafer was then baked at 200 °C for 1 min using the programmable hotplate and cooled to room temperature. On this wafer, approximately 40 μm thick SU-8 2035 was spin coated. The wafer was softbaked at 65 °C for 3 min and 95 °C for 15 min using the programmable hot plate. The exposure was performed using a maskless pattern generator (μPG101, Heidelberg Instruments, Heidelberg, Germany) at 17.5 mW laser power.

Subsequent spin coating, softbake and exposure were used on this wafer to create the semicircular pyramidal structures (figure 1(a)) of nominal thicknesses 80 μm, 120 μm, 160 μm, and 200 μm. Exposure powers of 17.5 mW, 21 mW, 28 mW, and 35 mW respectively were used to create these layers. An exposure power of 17.5 mW was found to be adequate to create both 40 μm and 80 μm layer thicknesses. The post exposure bake was performed by baking the wafer at 65 °C for 6 min and 95 °C for 35 min using the programmable hot plate and cooled to room temperature. The wafer was then developed using SU-8 developer (Microchem, Westborough, MA, USA).

Hidden subsurface structures (figure 1(b)) were fabricated on a separate borosilicate glass wafer coated with Omnicoat adhesion promoter using grayscale lithography. The hidden

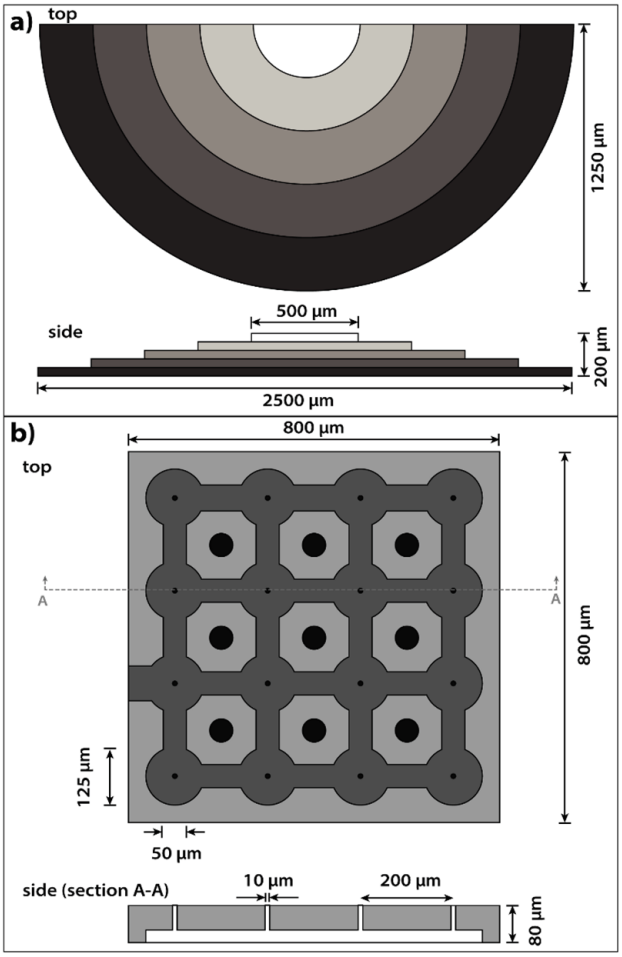

Figure 1. Schematic images of SU-8 microstructures. (a) Top view and side view of the five layered semicircular pyramidal structures. Each layer is roughly 40 μm thick. The width of the pyramid ranges from 2500 μm at the bottommost layer to 500 μm at the topmost layer in steps of 500 μm[3]. (b) Top view and side view image of the interconnected microwell structures fabricated using grayscale lithography. Microwells of 125 μm diameter are connected to each other with microchannels of width 50 μm. Microchannels and microwells are partially exposed using grayscale lithography to create subsurface features. There are also pores in the center of diameter 50 μm. Side view shows 10 μm microports inside the microwells and the total thickness of the design is 80 μm.

subsurface structures consisted of microwells, which are microfluidic reservoirs, interconnected by microchannels. The fluids in the microwells were designed to be dispersed through microports of diameter 10 μm through the center of the microwells. The diameter of the microwells were 125 μm and the width of the microchannels were 50 μm. The covers for these microchannels were fabricated using reduced laser power using grayscale lithography. The design also consisted of pores of 50 μm diameter in between adjacent microwells. Approximately 80 μm thick SU-8 2035 was spin coated on this wafer and softbaked at 65 °C for 5 min and 95 °C for 20 min. The hidden subsurface structures were fabricated by partially exposing the top cover of the channel with 50% of the total laser power of 17.5 mW and the surrounding area was exposed using 100% of the total laser power of 17.5 mW. The wafer was then postbaked at 65 °C for 5 min and 95 °C for 15 min and developed using the SU-8 developer for 30 min.

2.2. Fabrication of microstructures on silicon substrate

To test the applicability of this technique to other substrates, we fabricated microstructures on silicon wafers and characterized the dimensions using the autofluorescence emission images. A semicircular pyramid, like the design shown in figure 1(a), was fabricated on a silicon wafer using dry film sheets (SUEX®, DJ Microlaminates, Inc. Sudbury, MA, USA). These SU-8 sheets were deposited on the silicon wafer using a professional laminator (ProLam Ultra, Akiles Products, Inc. Mira Loma, CA, USA). All layers were deposited at 65 °C unless mentioned otherwise.

We fabricated SU-8 bridge structures, suspended on anchors, on silicon wafer (figure 2) using multilayer lithography with SU-8 sheets. The first SU-8 sheet of 125 μm nominal thickness was deposited on a silicon wafer using a professional laminator to fabricate anchor layer. This layer was exposed using the laser pattern generator at 70 mW laser power with a speed reduction factor of 4. The wafer was then postbaked at 65 °C for 10 min and 95 °C for 35 min and developed using SU-8 developer. A second SU-8 sheet of 40 μm nominal thickness was deposited on the same wafer, above the anchors at 50 °C using the professional laminator to create bridge layers. The temperature is kept at 50 °C to maintain the suspension and prevent flowing of the bridge layer during lamination. The wafer was exposed at 70 mW laser power with a speed reduction factor of 2. The post exposure bake was performed at 53 °C for 8 h. The wafer was then developed using SU-8 developer.

2.3. Fluorescence imaging

The autofluorescence emission of the SU-8 microstructures fabricated on both borosilicate glass wafers and silicon wafers was measured using an epi-fluorescence illuminator (Nikon Intensilight C-HGFI, Tokyo, Japan), an inverted microscope (Nikon Eclipse Ti-E, Tokyo, Japan), and a DAPI filter set (peak excitation wavelength of 365 nm; peak emission wavelength of 440 nm). Images were captured with a 10× objective and a microscope camera (Andor Zyla 5.5sCMOS, Abingdon, UK) with an exposure time of 30 s in a dark room to prevent interference from radiation in the visible spectrum. The resulting images were 16-bit grayscale maps of the autofluorescence emission intensities with a resolution of 2560 by 2160 pixels (0.65 μm/pixel). Multiple images were captured with Nikon Elements (Nikon, Tokyo, Japan) to statistically measure the degree of uncertainty.

[3] Reproduced from Rountree CM, Ramkumar PK, Saggere L. Novel imaging technique for non-destructive metrology and characterization of ultraviolet-sensitive polymeric microstructures. Review of Scientific Instruments. 1 March 2020;91(3):033710. [18], with the permission of AIP Publishing.

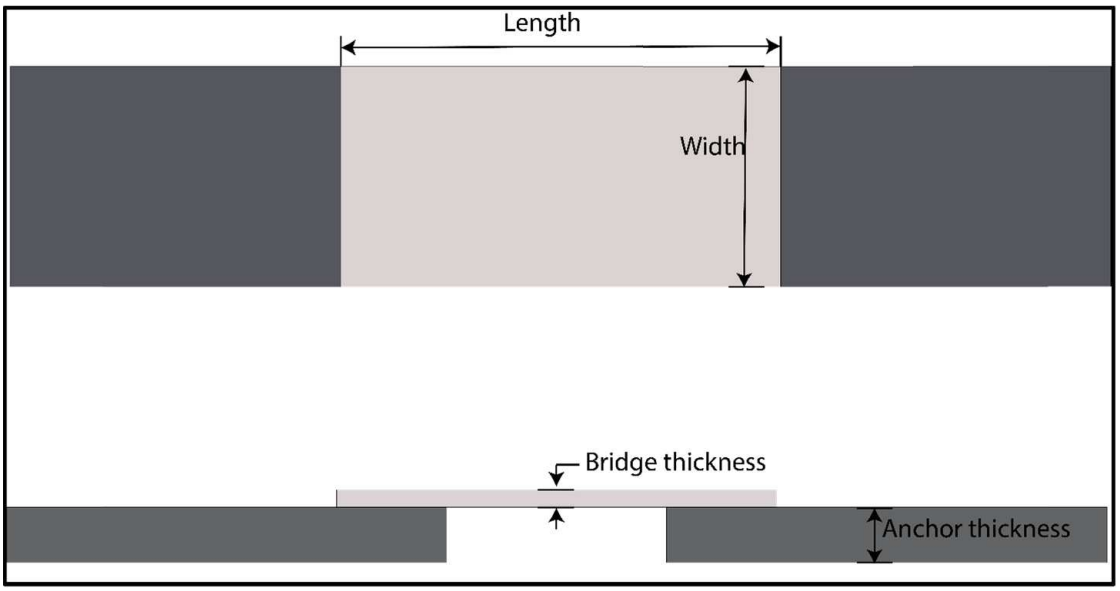

Figure 2. The top view (above) and the side view (below) of the bridge structures. The nominal thickness of the anchors and bridges are 125 μm and 40 μm, respectively. The width of the bridges and each anchor is 1000 μm. The annotated features on the bridges are characterized using the 2D depth profiles and validated using SEM.

2.4. Determination of feature size using SEM

The dimensions of the samples fabricated on borosilicate glass wafers were measured using SEM.(Hitachi S-3000N, Hitachi High Technologies America, Inc., Schaumburg, IL, USA). We also measured the dimensions of the structures fabricated on silicon wafers using SEM (JSM-IT500HR, JEOL Ltd, Tokyo, Japan). A thin layer (6 nm) of platinum–palladium was first sputter coated on the samples and then they were imaged using SEM at 5 kV accelerating voltage. The samples were tilted at 45° and 90° angles to directly measure the thicknesses of the different feature sizes. The feature sizes measured from SEM were compared with the pixel intensities of the samples measured in the previous step.

2.5. Creation of 2D depth profile and validation of the dimensions using SEM

The raw 16-bit autofluorescence emission images were imported into MATLAB (Mathworks, Natick, MA, USA) and converted into 2D depth profile images using custom MATLAB code. The relationship between the autofluorescence emission intensities and the actual SU-8 thicknesses was determined by measuring the average intensity of each distinct layer of the SU-8 semicircular pyramidal structure (figure 1(a)). The relationship between autofluorescence emission intensities and the corresponding SEM thickness was examined (see section 3). Using this equation, the SU-8 thickness (ℓ) can be determined based on the measured autofluorescence emission intensity (x) with the following fit parameters (a, b, c):

$$\ell = a\mathrm{e}^{bx} + c. \tag{1}$$

Coefficients:

$$\begin{aligned} a &= 93.4 \\ b &= 6.02 \times 10^{-5} \\ c &= -98.4 \\ R^2 &= 0.9968. \end{aligned}$$

Each raw 16-bit autofluorescence emission image was converted into a 2D depth profile by applying equation (1) on a pixel-by-pixel basis. The resulting 2D depth profile was spatially filtered using the algorithm of morphological opening-closing by reconstruction with a geodesic disk-shaped filter (15 pixel diameter) to remove the minor blemishes and debris that accumulated on the SU-8 samples during autofluorescence emission imaging.

Finally, we created 2D depth profiles of the structures fabricated on silicon wafers using the methodology described above. The thickness and lateral dimensions were then determined. We first determined the relationship between SU-8 thicknesses and the corresponding autofluorescence intensities of pyramidal structures fabricated on silicon wafers. Subsequently, we applied this relationship to bridge structures fabricated on silicon wafers and generated 2D depth profile images which was used to measure the dimensions of these structures. We then validated these dimensions using the SEM micrographs as part of blinded experiments. Both thickness and lateral dimensions were validated in these experiments.

Similar to equation (1), another fit was obtained for pyramidal structures fabricated on silicon wafers that related SU-8 thickness (ℓ) with autofluorescence emission intensities (x) as shown in equation (2)

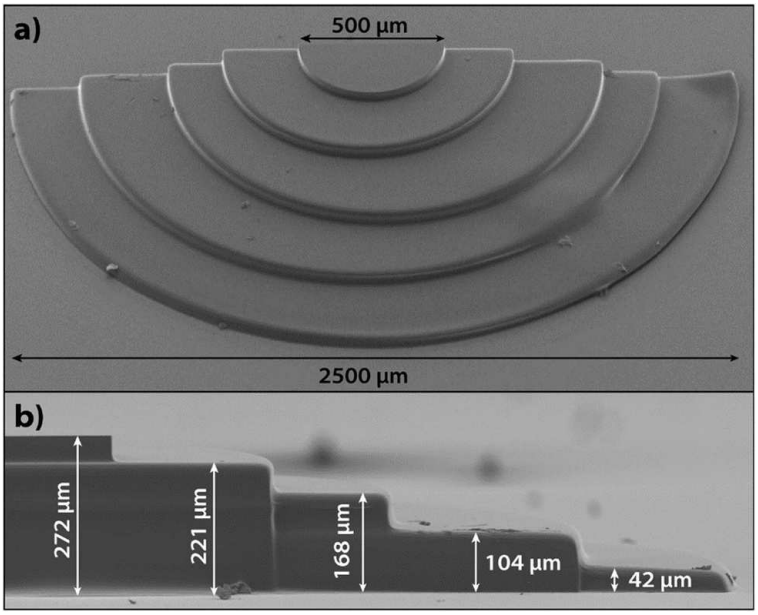

Figure 3. SEM characterization of the fabricated microstructures. (a) SEM micrograph of a five layer semicircular pyramidal structure captured using 45° tilt angle; (b) micrograph displaying the side view of the semicircular pyramidal structure captured using 90° tilt angle[4].

$$\ell = ae^{bx} + c. \tag{2}$$

Coefficients:

$$a = 161.7$$
$$b = 3.037 \times 10^{-5}$$
$$c = -165.8$$
$$R^2 = 0.9962.$$

The thickness and the lateral dimensions of the bridge structures obtained from the 2D depth profile were then validated by comparing it with their SEM micrographs. These validation characterizations were performed by operators in a blinded experiment. None of the operators was aware of the dimensions of the bridge structures. To validate the lateral dimensions, two operators characterized the length and width of the bridge structures (shown in figure 2) from the 2D depth profiles using ImageJ, an image processing software (ImageJ, NIH, USA). These results were compared with the lateral dimensions obtained from the SEM micrographs by two other operators who characterized the lengths and the widths of the bridge structures using SEM micrographs. To validate the thicknesses of the bridge structures obtained from 2D depth profile images, two operators characterized the thicknesses of bridges and thicknesses of anchors as annotated in figure 2. These results were compared to the thicknesses obtained from the 2D depth profiles of the bridge structures. There was no significant effect of operator on these measurements (ANOVA, $p > 0.05$) so results from the two operators were pooled in subsequent analysis.

[4] Reproduced from Rountree CM, Ramkumar PK, Saggere L. Novel imaging technique for non-destructive metrology and characterization of ultraviolet-sensitive polymeric microstructures. Review of Scientific Instruments. 1 March 2020;91(3):033710. [18], with the permission of AIP Publishing.

3. Results and discussion

In this section, we discuss the relationship between the autofluorescence emission intensities and the measured thicknesses using SEM. This exponential relation was used to generate 2D depth profiles that represent the thickness of different regions of the microstructure based solely on their autofluorescence emission intensities. We then describe the characterization of hidden subsurface features using this technique. Finally, we discuss the advantages and limitations of this technique to characterize surface and subsurface SU-8 features.

3.1. Autofluorescence emission of 3D SU-8 microstructures

To determine the relationship between SU-8 thickness and autofluorescence emission intensity, we designed and fabricated a multilayered, 3D SU-8 microstructure in the form of a semicircular pyramid with five different thicknesses (figures 1(a) and 3) and then measured the autofluorescence emission intensity via epi-fluorescence microscopy with a standard DAPI filter set (365 nm excitation/440 nm emission). Although spin speeds were selected to create a five layered pyramid in steps of 40 μm, the thicknesses from the second layer onwards varied considerably (figure 3(b)) from the intended total thickness of 80 μm, which was not unexpected.

The initial SU-8 layer was spun on a low friction, well-characterized glass wafer while all subsequent layers were spun on an existing SU-8 layer that had higher surface

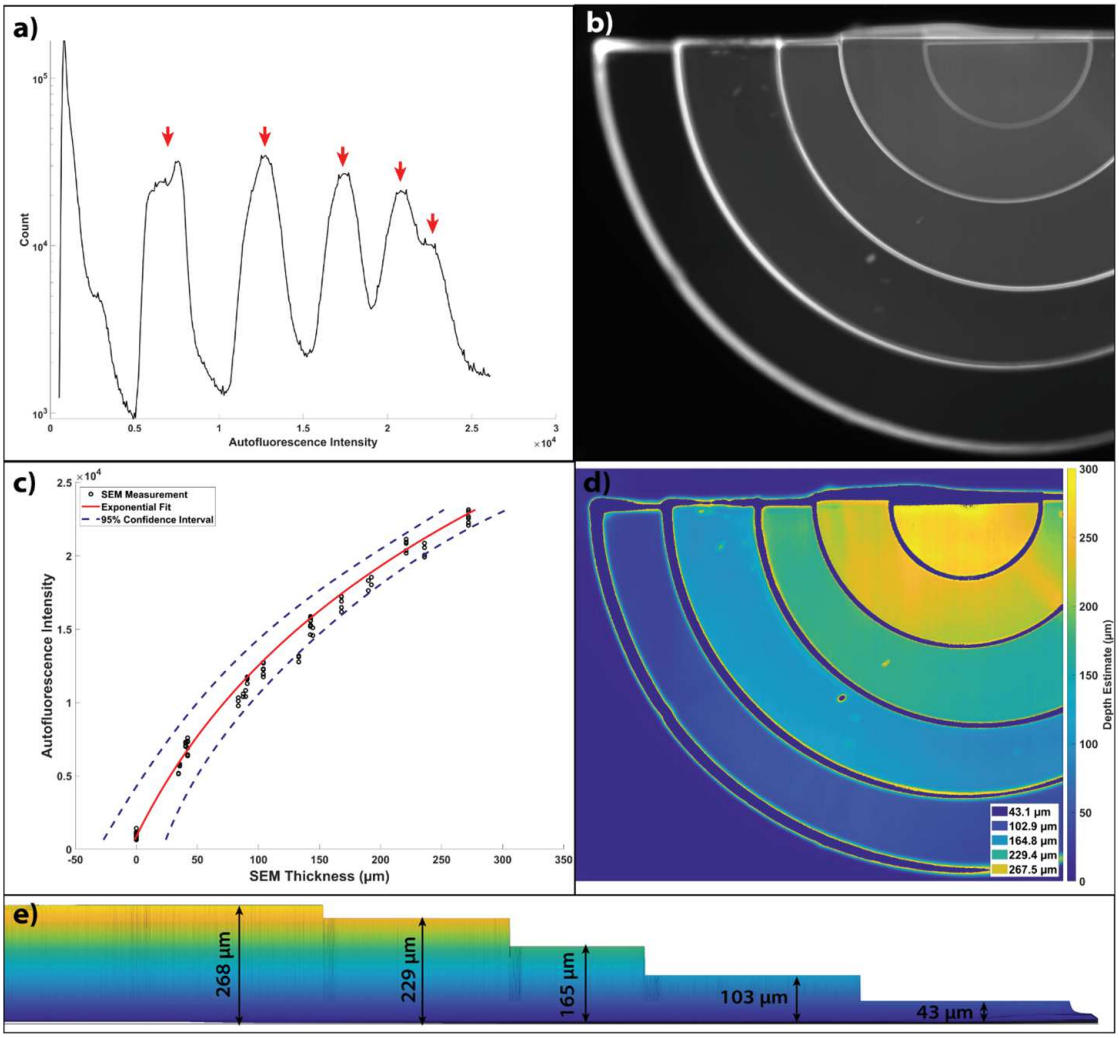

Figure 4. Autofluorescence emission characterization of the semicircular pyramidal structure. (a) Histogram showing the autofluorescence intensity vs pixel count which displays the five peaks (red arrows) corresponding to five different layers of the semicircular pyramid starting from the bottommost layer to the topmost layer. The initial large spike corresponds to the black background and is disregarded. The 5th peak is not as pronounced as the other peaks due to smaller area at the top and the general exponential nature of the autofluorescence emission. (b) Raw autofluorescence image captured using the inverted microscope at 10× objective showing autofluorescence emission at different layers of the semicircular pyramid fabricated on borosilicate glass wafer. (c) Autofluorescence intensity vs thickness of the individual layers of the semicircular pyramid. The thicknesses of the microstructures were measured using SEM. The resulting exponential curve (red line; dashed blue lines indicate 95% confidence interval) was found to be a good fit with $R^2 = 0.9968$; (d) 2D Depth profile created using the generated expression from (c). Different colors represent different thicknesses as represented by the side bar. (e) 2D depth profile of the side view of the semicircular pyramidal structure.

irregularities resulting in the observed thicker SU-8 layers. Fluorescence imaging (figure 4(b)) showed that each SU-8 layer of the pyramid emitted a distinct level of autofluorescence, which was monotonically related to the thicknesses of SU-8 (figure 4(c)). When presented in histogram form (figure 4(a)), well-defined peaks corresponding to each of the five layers of the SU-8 pyramid can be observed. These autofluorescence emission data were found to be well fit (figure 4(c); $R^2 = 0.9968$) with an exponential calibration equation (equation (1)) derived from Beer–Lambert's Law. Using this equation on a pixel-by-pixel basis with the autofluorescence emission image (figure 4(b)), we could create a 2D depth profile for the pyramidal microstructure by estimating the thickness at each pixel (figure 4(d)). Table 1 shows the measurement comparisons between the autofluorescence emission technique and SEM. From table 1, it is evident that the resulting depth profile closely matched with measurements obtained through SEM imaging (figure 3(b)). The 3D reconstructed side profile of the depth profile is shown in figure 4(e).

Although previous research has identified a monotonic relationship between SU-8 thickness and autofluorescence emission intensity, these studies have specifically focused on methods for reducing SU-8's autofluorescence emission

Table 1. Thickness error between the autofluorescence measurement technique and SEM for the five layered pyramidal structure on borosilicate glass.

	Thickness measured using 2D depth profiles (μm)				Autofluorescence Intensity	
Thickness measured using SEM (μm)	Mean $\pm$ SD	25% and 75% quartiles	% error	95% confidence Intervals (μm)	Mean $\pm$ SD	25% and 75% quartiles
42	43.1 $\pm$ 4.3	38.5–46.4	2.6	32.4–53.9	6906 $\pm$ 507	6361–7284
104	102.9 $\pm$ 5.0	98.7–108.1	1.1	90.4–115.4	12 760 $\pm$ 409	12 408–13 183
168	164.9 $\pm$ 7.1	158.6–170.3	1.8	153.3–176.3	17 213 $\pm$ 453	16 816–17 557
221	229.4 $\pm$ 7.3	222.2–233.8	3.8	218.6–240.2	20 859 $\pm$ 371	20 491–21 082
272	267.5 $\pm$ 9.1	259.6–276.2	1.7	251.9–283.1	22 685 $\pm$ 413	22 324–23 075

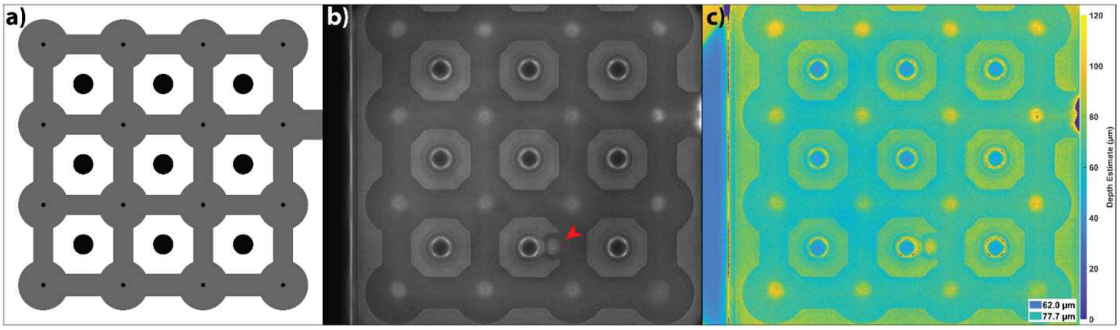

Figure 5. Metrology and characterization of the interconnected microwell array using the expression generated from the previous results. (a) Grayscale bitmap image of the exposed design showing circular microwells containing hollow micro pores at their centers interconnected to each other using microchannels. The microwells and microchannels are partially exposed to create hidden subsurface features. At the center of every four microwells are fully exposed hexagonal pads with a circular central pore of 50 μm diameter. (b) Autofluorescence emission of the interconnected microwell array fabricated on borosilicate glass wafer. The fully exposed regions have higher intensities than the partially exposed regions. A fabrication error is highlighted by the red arrow. (c) 2D depth profile of the hidden microwell array generated with the help of equation (1). The thicknesses of different regions can be determined using the side legend. The fully exposed region is roughly 80 μm thick and the partially exposed region is roughly 62 μm thick.

[9, 11, 12] and, to our knowledge, there are no models in the literature that relate autofluorescence to SU-8 thickness measurement for metrology purposes. However, other groups [13, 14] have used a variant of Beer–Lambert's Law (equation (1)) incorporating a term accounting for fluorescent emission to characterize the thicknesses of fluorophore-doped thin films and this equation works equally well for autofluorescence materials as evidenced by the good fit we observed. These results also agree well with previous autofluorescence emission measurements of SU-8, which appear to follow the general shape of an exponential association curve [11, 15] similar to our data, but it is difficult to make direct comparisons due to differences in excitation intensity, microscope camera gain, and other factors.

3.2. *Identification of hidden subsurface SU-8 topologies*

The key advantage of fluorescence imaging for SU-8 metrology is the identification and measurement of complex 3D microstructures containing hidden subsurface features such as microchannels or microwells since these features are difficult to observe with conventional metrology techniques without destructive testing. By measuring emitted fluorescent light radiation from SU-8 samples, as opposed to the reflected light measured by SEM and optical profilometry, fluorescent imaging is capable of non-destructive measurements of hidden SU-8 microstructures even if they are *in-situ* on the fabrication wafer. To explore the potential of this technique, we used grayscale photolithography to fabricate an enclosed microwell array (figure 5(a)) in a single step exposure. When the resulting microstructure was fluorescently imaged (figure 5(b)) following fabrication, clear contrast differences were observed between the full thickness regions (high intensity) and the partial thickness of the enclosed microwells (lower intensity). Since this microstructure is fully enclosed, it was impossible to non-destructively measure the thicknesses of the hidden microwell array using SEM but the 2D depth profile produced from autofluorescence emission imaging (figure 5(c)) clearly shows that the microwell cover was approximately 64 μm, which matches up well with our expectations. The high contrast differences observed between different SU-8 thicknesses also allows quick and easy identification of fabrication errors such as the fabrication defect highlighted in red in figure 5(b). However, these high contrast differences also make it difficult to observe very small features such as the 10 μm diameter microports at the center of each microwell, which appear as diffuse bright spots.

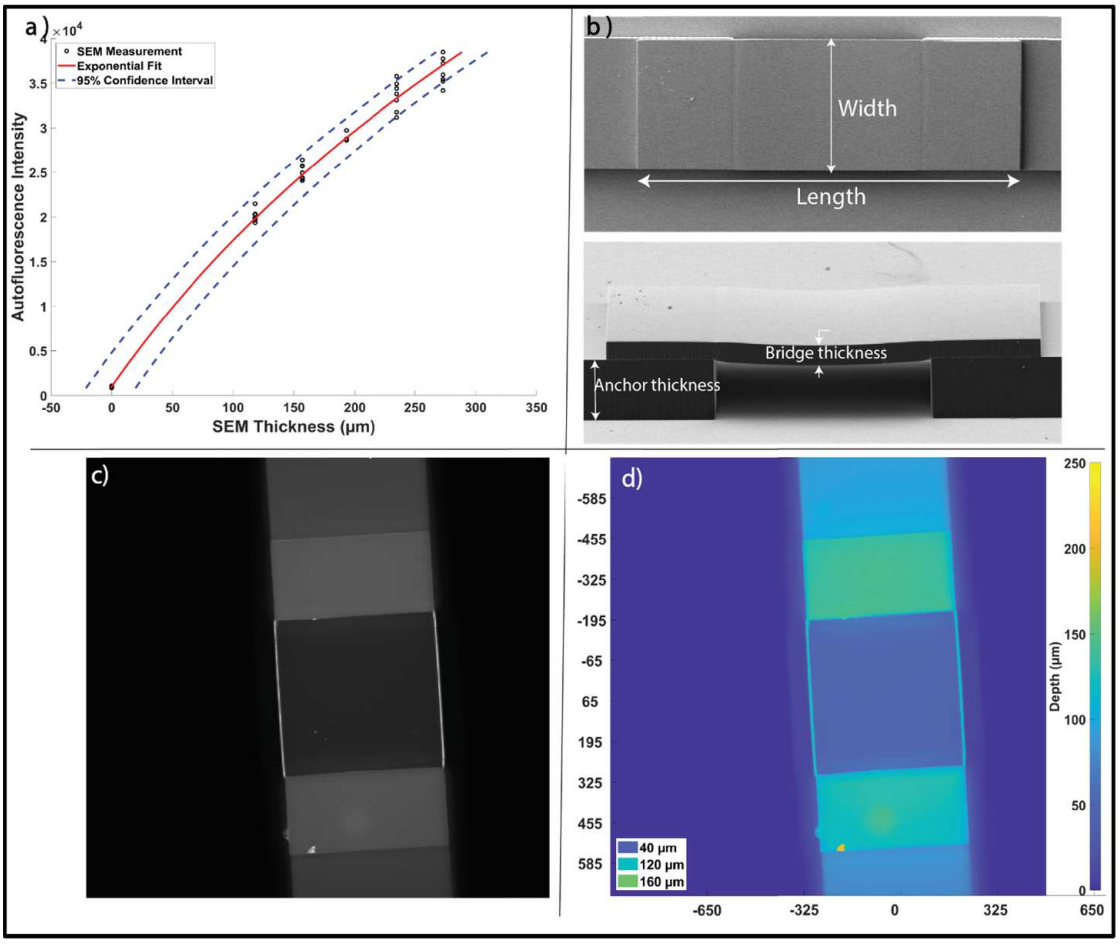

Figure 6. The calibration curve on silicon wafer and the bridge structures used for validation of lateral and thickness dimensions. (a) The autofluorescence intensity vs thickness of the individual layers of the semicircular pyramid fabricated on silicon wafer. The thicknesses of the microstructures were measured using SEM. The resulting exponential curve (red line; dashed blue lines indicate 95% confidence interval) was found to be a good fit with $R^2 = 0.9968$. (b) SEM micrograph of the top view (above) of the bridge structure and the micrograph displaying the side view (below) of the bridge structure suspended on anchors captured using 90° tilt angle. There is a slight depression at the center of the bridges caused due to surface tension effects of the developer as observed in the side view of bridge micrograph. (c) Raw autofluorescence image captured using the inverted microscope at 10× objective showing autofluorescence emission at different layers of the bridge structure fabricated on silicon wafer. (d) 2D depth profile of the suspended bridge structure generated with the help of equation (2). The thicknesses of different regions can be determined using the side legend. The thickness of the bridge structure is estimated to be about 40 μm and the thickness of the anchor structures is estimated to be about 119 μm.

Table 2. Validation of the lateral dimensions of the bridge structures from blinded experiments.

	Measured using SEM micrographs (μm)		Measured using 2D depth profiles (μm)			
Dimension of the bridge	Mean ± SD	25% and 75% quartiles	Mean ± SD	25% and 75% quartiles	% error	95% confidence intervals of the 2D depth profile measurements (μm)
Length	1013.50 ± 34.76	997.09–1034.69	1002.4 ± 2.44	1001.41–1003.42	1.09	1001.33–1003.47
Width	509.01 ± 16.50	502.55–516.50	500.01 ± 2.98	498.56–502.14	1.76	498.7–501.32

3.3. Calibration of the technique with silicon substrate and validation of lateral and thickness dimensions of the bridge structures

We calibrated the autofluorescence emission technique on a pyramidal structure fabricated on a silicon wafer and obtained a relationship between the autofluorescence emission intensity and the thickness of the pyramidal steps as shown in figure 6(a). From this figure, we can see that the autofluorescence emission data were found to be well fit ($R^2 = 0.9962$) with an exponential calibration equation (equation (2)) derived from Beer–Lambert's Law. While the general behavior of the two curves shown in figures 4(c) and 6(a) are the same,

Table 3. Validation results of the thicknesses of the bridge structures suspended on anchors from blinded experiments.

Dimension of the suspended bridge struct.	Measured using SEM micrographs (μm)		Measured using 2D depth profiles (μm)		% error	95% confidence intervals of the 2D depth profile measurements (μm)	Autofluorescence intensity	
	Mean $\pm$ SD	25% and 75% quartiles	Mean $\pm$ SD	25% and 75% quartiles			Mean $\pm$ SD	25% and 75% quartiles
Bridge thickness	38.97 $\pm$ 1.12	38.80–40.06	41.0 $\pm$ 2.6	39.2–43.2	5.2	38.8–43.3	8088 $\pm$ 410	7798–8440
Anchor thickness	118.09 $\pm$ 1.8	118.77–120.64	118.8 $\pm$ 3.4	115.8–122.1	0.6	116.7–120.9	18 603 $\pm$ 398	18 250; 18 977

the difference in their respective coefficients, as shown in equations (1) and (2), can be attributed to the opaqueness of the silicon wafer. Unlike borosilicate glass wafers, silicon wafers reflect all the incident radiation during the fluorescence imaging, and as a result the autofluorescence intensities of the microstructures are higher when compared to those fabricated on borosilicate glass wafers.

We used bridge structures suspended on anchors to validate the dimensions obtained using the 2D depth profiles. Figure 6(b) shows the representative micrograph of the top view of the bridge structure, and the side view obtained by tilting the stage to about 90° during SEM imaging to facilitate the thickness measurements. From the side view, a small depression of the bridge structure can be observed caused due to surface tension effects during the photoresist development stage of the microfabrication. Figure 6(c) shows the top view of the autofluorescence emission image of the suspended bridge structure. Clear contrast differences corresponding to different thicknesses of the bridge and anchors can be observed from this image. Also, the effects of depression of the bridges are seen as bright lines on the autofluorescence emission image, and its 2D depth profile image shown in figure 6(d). The 2D depth profile of the same bridge structure depicts the thicknesses of the bridge structures and the anchors, whose dimensions are represented on the colored legends.

The thicknesses and the lateral dimensions of the suspended bridge structures were validated using the SEM micrograph as part of blinded experiments. A total of ten bridge structures were analyzed. The results from the two different human operators were pooled because there was no statistically significant effect of operator ($p > 0.05$; ANOVA test). Table 2 shows the comparison of the lateral dimensions obtained using SEM and the 2D depth profile images. From the error margins, we can see that the lateral dimensions obtained using the autofluorescence emission technique closely matched with those obtained using SEM. Table 3 shows the comparison of the thickness dimensions of the bridges and anchors obtained using SEM and the 2D depth profile images. The anchor thicknesses obtained using autofluorescence emission technique closely matched with that obtained using SEM. A relatively higher error margin of 5.2% was recorded from the comparison of the values of the bridge thicknesses obtained using the autofluorescence emission technique and the SEM. This could be partially attributed to the slight curvature of the bridge, which might have caused some variation in the autofluorescence measurements since they were averaged across the entire span of the bridge. Despite this error margin, the absolute difference in means between the two techniques was only 2 μm and within the standard deviation of the autofluorescence measurements.

3.4. Advantages and limitations of fluorescence imaging of SU-8 metrology

Autofluorescence emission imaging offers several unique advantages over existing metrology methods for identifying and measuring the thicknesses of SU-8 microstructures. First, it allows completely non-destructive measurement of SU-8 samples facilitating the identification and quantification of fabrication defects, multilayered 3D microstructures, and hidden features such as microchannels and microwells. Second, since the technique measures emitting autofluorescence of SU-8, it can be accomplished *in-situ* on the wafer immediately following fabrication without any sample preparation, dyes, or releasing the microstructure. Finally, it is a quick and relatively low-cost alternative to current SU-8 metrology methods since it only requires a fluorescent microscope, a DAPI filter-set, and a microscope camera.

While autofluorescence emission provides an accurate methodology for dimensional characterization, there are some limitations. Prolonged high intensity UV stimulation can photobleach the samples and, as a result, cause inaccurate measurements [15–17]. Moreover, devices with smaller footprints can be harder to measure because of the edge effect as observed in figure 5(b). However, higher resolution imaging of smaller features can be accomplished using higher microscope magnifications at the cost of a substantial reduction in the image field of view. Finally, this methodology needs to be validated for other UV sensitive polymers as well as other grades of SU-8. Further work is needed to fully explore the advantages and applications of SU-8 fluorescent imaging, but these results demonstrate that it can be an effective yet economical alternative to existing metrology methods.

4. Conclusions

In this study, we have established an accurate new methodology for the metrology and characterization of SU-8 microstructures using the autofluorescence emission intensity. We have demonstrated that this technique can be used to measure a variety of SU-8 microstructures including hidden subsurface microstructures. We have also validated the results obtained from our technique using SEM. Unlike the commonly used characterization techniques like SEM, our methodology is non-destructive, cost effective, and can measure different features in a 3D SU-8 microstructure. The generated depth profile images based on the relationship between the thickness of the fabricated microstructures and emitted autofluorescence emission intensity are demonstrated to be highly reliable and reproducible. Further work is needed to determine the application of this technique to microstructures fabricated using other polymer materials.

Acknowledgments

This work made use of instruments in the Electron Microscopy Core of UIC's Research Resources Center and the authors would like to thank Olivia Thomson for her assistance in gathering the SEM images. This work was supported by the National Science Foundation under Grant No. 1840145 and the National Institutes of Health under Grant No. 5R21EB028069-02 and Grant No. R01NS113935. Any opinions, findings, and conclusions or recommendations expressed in this material are those of the authors and do not necessarily reflect the views of the National Science Foundation or the

National Institutes of Health. We would like to acknowledge Dr John B. Troy for his helpful suggestions. We would like to acknowledge excellent technical assistance from Mr Sai-Siva Kare, Ms Kira Jeffris, Mr Ian Jones, and Ms Angela Mitevska.

ORCID iDs

Pradeep Kumar Ramkumar https://orcid.org/0000-0003-3297-4996
Corey M Rountree https://orcid.org/0000-0003-3298-0560
Laxman Saggere https://orcid.org/0000-0001-6429-6240
John D Finan https://orcid.org/0000-0003-4626-9702

References

[1] Lorenz H, Despont M, Fahrni N, LaBianca N, Renaud P and Vettiger P 1997 SU-8: a low-cost negative resist for MEMS *J. Micromech. Microeng.* **7** 121
[2] Lee J B, Choi K H and Yoo K 2015 Innovative SU-8 lithography techniques and their applications *Micromachines* **6** 1–8
[3] Arscott S 2014 SU-8 as a material for lab-on-a-chip-based mass spectrometry *Lab Chip* **14** 3668–89
[4] Chaudhri B P, Ceyssens F, De Moor P, Van Hoof C and Puers R 2010 A high aspect ratio SU-8 fabrication technique for hollow microneedles for transdermal drug delivery and blood extraction *J. Micromech. Microeng.* **20** 064006
[5] Altuna A *et al* 2013 SU-8 based microprobes for simultaneous neural depth recording and drug delivery in the brain *Lab Chip* **13** 1422
[6] Cao C, Birtwell S W, Høgberg J, Morgan H, Wolff A and Bang D D 2012 Gold nanoparticles-coated SU-8 for sensitive fluorescence-based detections of DNA *Diagnostics* **2** 72–82
[7] Cao C, Birtwell S W, Høgberg J, Wolff A, Morgan H and Bang D D 2011 Surface modification of photoresist SU8 for low autofluorescence and bioanalytical applications *15th Int. Conf. on Miniaturized Systems for Chemistry and Life Sciences* 2 October (Chemical and Biological Microsystems Society) pp 1161–3
[8] Walczak R A, Sniadek P and Dziuban J A 2011 SU-8 photoresist as material of optical passive components integrated with analytical microsystems for real-time polymerase chain reaction *Opt. Appl.* **41** 873–84
[9] Marie R, Schmid S, Johansson A, Ejsing L, Nordström M, Häfliger D, Christensen C B, Boisen A and Dufva M 2006 Immobilisation of DNA to polymerised SU-8 photoresist *Biosens. Bioelectron.* **21** 1327–32
[10] Rammohan A, Dwivedi P K, Martinez-Duarte R, Katepalli H, Madou M J and Sharma A 2011 One-step maskless grayscale lithography for the fabrication of 3-dimensional structures in SU-8 *Sensors Actuators* B **153** 125–34
[11] Wang L, Wu Z Z, Xu B, Zhao Y and Kisaalita W S 2009 SU-8 microstructure for quasi-three-dimensional cell-based biosensing *Sensors Actuators* B **140** 349–55
[12] Grimaldi I A, Testa G, Persichetti G, Loffredo F, Villani F and Bernini R 2016 Plasma functionalization procedure for antibody immobilization for SU-8 based sensor *Biosens. Bioelectron.* **86** 827–33
[13] Jones A C, Millington M, Muhl J, De Freitas J M, Barton J S and Gregory G 2001 Calibration of an optical fluorescence method for film thickness measurement *Meas. Sci. Technol.* **12** N23
[14] Hagemeier T, Hartmann M, Kühle M, Thévenin D and Zähringer K 2012 Experimental characterization of thin films, droplets and rivulets using LED fluorescence *Exp. Fluids* **52** 361
[15] Pardon G, Saharil F, Karlsson J M, Supekar O, Carlborg C F, Van Der Wijngaart W and Haraldsson T 2014 Rapid mold-free manufacturing of microfluidic devices with robust and spatially directed surface modifications *Microfluid Nanofluidics* **17** 773–9
[16] Roth S, Hadass O, Cohen M, Verbarg J, Wilsey J and Danielli A 2019 Improving the sensitivity of fluorescence-based immunoassays by photobleaching the autofluorescence of magnetic beads *Small* **15** 1803751
[17] Schleusener J, Lademann J and Darvin M E 2017 Depth-dependent autofluorescence photobleaching using 325, 473, 633, and 785 nm of porcine ear skin ex vivo *J. Biomed. Opt.* **22** 091503
[18] Rountree C M, Ramkumar P K and Saggere L 2020 Novel imaging technique for non-destructive metrology and characterization of ultraviolet-sensitive polymeric microstructures *Rev. Sci. Instrum.* **91** 033710